Predictive radiomics signature for treatment response to nivolumab in patients with advanced renal cell carcinoma

Eoghan R. Malone, MD[1]; Hao-Wen Sim, MD[1]; Audrius Stundzia, MD[2]; Sacha Pierre, MD[4]; Ur Metser, MD[5]; Martin O'Malley, MD[4]; Adrian G. Sacher, MD[1,3]; Srikala S. Sridhar, MD[1,3]; Aaron R. Hansen, MD[1,3]

[1]Division of Medical Oncology and Hematology, Princess Margaret Cancer Centre, UHN, Toronto, ON, Canada; [2]Tomographix IP Ltd., Toronto, ON, Canada; [3]Department of Medicine, University of Toronto, Toronto, ON, Canada; [4]Division of Abdominal Imaging, Joint Department of Medical Imaging, University of Toronto, Toronto, ON, Canada; [5]Division of Molecular Imaging, Joint Department of Medical Imaging, University of Toronto, Toronto, ON, Canada

Cite as: Malone ER, Sim H-W, Stundzia A, et al. Predictive radiomics signature for treatment response to nivolumab in patients with advanced renal cell carcinoma. *Can Urol Assoc J* 2022;16(2):E94-101. http://dx.doi.org/10.5489/cuaj.7467

Published online September 24, 2021

Abstract

Introduction: The anti-programmed cell death protein-1 (PD-1) immune checkpoint inhibitor nivolumab is currently approved for the treatment of patients with metastatic renal cell carcinoma (mRCC); approximately 25% of patients respond. We hypothesized that we could identify a biomarker of response using radiomics to train a machine learning classifier to predict nivolumab response outcomes.

Methods: Patients with mRCC of different histologies treated with nivolumab in a single institution between 2013 and 2017 were retrospectively identified. Patients were labelled as responders (complete response [CR]/partial response [PR]/durable stable disease [SD]) or non-responders based on investigator tumor assessment using RECIST 1.1 criteria. For each patient, lesions were contoured from pre-treatment and first post-treatment computed tomography (CT) scans. This information was used to train a radial basis function support vector machine classifier to learn a prediction rule to distinguish responders from non-responders. The classifier was internally validated by a 10-fold nested cross-validation.

Results: Thirty-seven patients were identified; 27 (73%) met the inclusion criteria. One hundred and four lesions were contoured from these 27 patients. The median patient age was 56 years, 78% were male, 89% had clear-cell histology, 89% had prior nephrectomy, and 89% had prior systemic therapy. There were 19 responders vs. eight non-responders. The lesions selected were lymph nodes (60%), lung metastases (23%), and renal/adrenal metastases (17%). For the classifier trained on the baseline CT scans, 69% accuracy was achieved. For the classifier trained on the first post-treatment CT scans, 66% accuracy was achieved.

Conclusions: The set of radiomic signatures was found to have limited ability to discriminate nivolumab responders from non-responders. The use of novel texture features (two-point correlation measure, two-point cluster measure, and minimum spanning tree measure) did not improve performance.

Introduction

Immunotherapies have revolutionized the treatment of metastatic renal cell carcinoma (mRCC) and have demonstrated improved overall survival (OS).[1-4] Despite this advance, not all patients benefit from immune treatments and to date, no predictive biomarker has been validated. CheckMate 025 was a landmark, randomized, phase 3 trial that assigned patients with previously treated mRCC to the programmed cell death protein-1 (PD-1) inhibitor nivolumab or everolimus. Patients treated with nivolumab had a statistically significant improvement in OS of approximately five months compared with everolimus;[1] however, the objective response rate to nivolumab was 25%, suggesting that this benefit was limited to a small proportion of patients. Furthermore, higher levels of PD-L1 expression did not predict for responses. A predictive biomarker would facilitate selection of patients most likely to respond to nivolumab and allow those who are not likely to respond to avoid immune-related adverse events and reduce the substantial treatment-related costs.

The application of radiomics technology in medical imaging offers a potential platform to develop a predictive signature.[5,6] Radiomics extracts quantitative information from routine radiological images to identify characteristic features that could predict tumor biology and immune cell infiltrates. Compared with biopsy-based methods, radiomics affords unique advantages: 1) it captures spatial information encompassing the entire tumor and microenvironment, thereby accounting for intra-tumoral heterogeneity and tumor-host interactions; 2) multiple lesions can be assessed in parallel, thereby accounting for inter-tumoral heterogeneity; 3) lesions can be assessed longitudinally for changes over time; and 4) unlike biopsies, it is a non-invasive method that presents minimal risk to patients.

The Predictive RadiOMIcs SignaturE for treatment response to nivolumab or PD-1/PD-L1 inhibitors in patients with advanced renal cell carcinoma (PROMISE) was a pilot

study that aimed to develop a radiomics signature to predict response to immune checkpoint inhibitors (ICI) in mRCC. We hypothesized that in patients with mRCC, host immune recognition of tumor cells would create a microenvironment of infiltrating immune effector cells. The microenvironment could predict for response to nivolumab and would have a distinct appearance on computed tomography (CT) images that could be captured using radiomics methods and subsequently developed into a predictive signature with clinical utility.

Methods

Patient selection

This single-institution, retrospective study of CT-derived textual features of patients diagnosed with mRCC between 2013 and 2017 was reviewed and approved by the local institutional ethics board (17-5340). Patients must have had histologically proven mRCC (any histology), received nivolumab, and had pre- and post-treatment CT scans. Patients were excluded if appropriate CT images were not available for analysis.

Image acquisition

Contrast-enhanced CT imaging of the thorax, abdomen, and pelvis was performed with non-ionic intravenous contrast. Regions of interest (ROI) were drawn circumferentially around each index lesion by a study member (HWS and SP). Each target lesion on CT imaging was assessed as a distinct entity to account for inter-tumoral heterogeneity. Responses were dichotomized into responders vs. non-responders based on RECIST version 1.1 measurements of the target lesion only.[7] Responders were defined as lesions with complete response (CP), partial response (PR), or stable disease (SD) for at least 12 weeks. Non-responders were defined as lesions with stable disease for less than 12 weeks, or progressive disease. The best response was used, such that patients with initial progressive disease, but treated beyond progression with subsequent treatment benefit, were regarded as responders. The decision to differentiate SD at 12 weeks was based on a study of response heterogeneity with immune checkpoint inhibitors.[8]

Radiomics analysis

Using computational algorithms, quantitative radiomics features were extracted from each contoured target lesion. These radiomics features represent the defining quantitative characteristics of the lesion. For the algorithms, each image voxel (a value on a regular grid in three-dimensional [3D] space) was quantized to a finite range of 32 grey levels. Additionally, algorithms initially described for two-dimensional (2D) pictures were adapted for 3D volumes, by extrapolating from the four principal directions in 2D to the 13 principal directions in 3D.[9]

For each tumor volume of interest (VOI), a set of 11 and 142 first- and second-order, and two-point correlation, two-point cluster, and minimum spanning tree texture metrics were generated. A set of 2D ROIs was used to construct a VOI that occupied a contiguous range of slices and overlapped from one slice to the next. The first-order metrics were composed of 11 image intensity percentiles from each VOI, ranging from the minimum value (0%) to the maximum value (100%) broken up into nine 10% intervals. Characterization of the one-dimensional image intensity histogram shape was provided by these metrics.

The intensities within each VOI were grouped into 32 equal-sized bins extending across the range of image intensities from the first percentile at the bottom, and the 99th percentile at the top prior to computing the 142 second-order texture metrics. The second order texture features were composed of metrics from four classes calculated from multidimensional histograms: 1) the mean and range of the 13 Haralick features computed from the gray scale co-occurrence matrix[10] taken over all 13 neighbor orientations;[9] 2) five features based on the neighborhood gray tone difference matrix;[11] 3) 10 features from the gray level run-length matrix;[12] and 4) the same 10 features from the gray level size zone matrix.[13] A detailed, illustrated description of these metrics has been previously published.[9]

Machine learning algorithm

A support vector machine (SVM) algorithm with a radial basis function (RBF) kernel was used to carry out all machine learning. A classifier was trained to predict pre-treatment whether advanced renal carcinoma tumors treated with nivolumab would be responders (CR/PR/durable SD) or non-responders and distinguish post-treatment between nivolumab responding and non-responding tumors, based on the texture features extracted from the associated VOIs. The MATLAB interface to the library for support vector machines (LibSVM) software library[14] was used to apply the SVM training algorithm to the data, consisting of 104 contoured lesions (lymph nodes: 62; lung metastases: 24; kidney or adrenal metastases: 18) from 27 patients, in these two configurations. It was necessary to tune three hyperparameters governing the behavior of the classifier for each SVM training run. The first hyperparameter was related to feature selection; 191 input texture features were ranked in order of their association with the response classification using an F-statistic approach.[15] A tunable hyperparameter, which represented the fraction of the most highly associated

features to keep, was applied to select the features that were used. The second hyperparameter was the standard cost parameter common to all versions of SVM, while the third was the width of the Gaussian that makes up the RBF kernel.

The three hyperparameters were tuned using a nested cross-validation scheme while ensuring to keep the assessment of accuracy totally independent. In each of 100 iterations of the outer loop, 10-fold cross-validation was used to hold out 10% of the data for testing, while the remaining 90% was passed to the inner loop. Within the inner loop, a further 10-fold cross-validation protocol was employed for each point in a 3D grid covering a range of fractions of the best features to retain, values of the SVM cost parameter, and values of the RBF width. For each grid point searched, the inner-loop cross validation result was recorded; the best performing triplet of hyperparameters was used to train a classifier using all of the inner-loop data. This classifier was then applied to classify the held-out data from the outer loop, and the results were recorded as the s accuracy.

The pre- and post-treatment texture features for each series, along with their binary classifications (non-responder: 0; responder: 1), were separately inputted into the second stage supervised machine learning (SML) RBF SVM classifier to train binary discrimination between the responders and non-responders. A nested 10-fold cross-validation protocol was used to assess classifier accuracy. The second stage SML algorithms used were also "as is," the same as were used for previous projects. The SVM algorithms generate a cross-validation (CV) accuracy value for each combination of three metaparameters: fraction, cost, and gamma, yielding a 3D CV accuracy space. The optimization target was to find the region of the parameter space yielding the highest CV accuracy.

Receiver operating characteristic and other post-hoc analyses

A SVM classifier produces a single, continuous number on the real line rather than a dichotomous binary classification as its output. The SVM classifier is only transformed into a classification when a threshold is applied to it. As a result, it is possible to adjust the threshold to adjust sensitivity and specificity, thereby creating a receiver operating characterist (ROC) curve. Repeating the outer loop of the nested cross-validation protocol 100 times yields 100 such numbers for each tumor; this results in a more fine-grained ROC curve than would be possible without repetitions. Each of the 100 numbers for a particular tumor represents an instance in which it was held out during cross-validation with a different 10% of the data, allowing for a more robust characterization of the accuracy for that case. In the results section below, the mean ± standard deviation (SD) accuracies reported are the best from each of the 100 ROC curves, and the sensitivities and specificities are taken from the point on each curve where the best accuracy was found. By combining all the trial data into a single curve, the ROC curves presented in the figures are generated.

Statistical analysis

Descriptive statistics were used to summarize baseline demographics. Survival estimates were computed using the Kaplan-Meier (KM) method. The accuracy of the predictive signature from the SVM classifier was determined by 10-fold nested cross-validation, and reported in terms of sensitivity, specificity, and area under the curve (AUC). An AUC of 0.5 would signify no discriminatory ability, 0.7–0.8 represents an acceptable level, 0.8–0.9 represents a good level of discrimination, and 0.9–1.0 would be excellent. Statistical significance was determined by permutation testing.[16] For permutation testing, the observed accuracy was compared against the distribution of accuracies obtained by random noise, generated by randomly labelling the radiomics signatures as being responders or non-responders using 10 000 permutations. Significance level was set at 0.05.

Results

Patients

Thirty-seven patients were identified between August 21, 2013 and October 6, 2017. Only 27 patients met the inclusion criteria with available imaging. Ten patients were excluded, as imaging was either not available (n=3) or the imaging protocol used was incompatible with the radiomics software (n=7). A final cohort of 27 patients were used for analysis. The median patient age was 56 years, 78% were male, 89% had clear-cell histology, 89% had prior nephrectomy, and 89% had prior systemic therapy. The selected patients were categorized as being in the good (30%), intermediate (60%), or poor (10%) risk groups as per the International Metastatic RCC Database Consortium (IMDC) scoring system.[17] The lesions selected were lymph nodes (60%), lung metastases (23%), and renal/adrenal metastases (17%). The characteristics of the patient population and ROIs are listed in Table 1.

The median progression and OS for the entire population were 10.8 months (range 1.4–48.8) (Fig. 1A) and 26.2 months (range 3.1–72.5) (Fig. 1B), respectively. For the responders and non-responders, the median progression-free survival (PFS) and OS were 14 months (range 3.5–48.8) (Fig. 2A) vs. 3.7 months (range 1.4–13.2) (Fig. 2B) ($p<0.0001$), and 28.8 months (range 3.7–72.5) (Fig. 3A) vs. 16.3 months (range 3.1–40.8) (Fig. 3B) ($p=0.13$), respectively.

The final data set of 27 subjects with pre-treatment and immune checkpoint inhibitor post-treatment yielded 52 responding lesions and 52 non-responding lesions that were

Table 1. Characters of the patients and ROIs

Patients identified: 37		
Included in study		27 (73)
Excluded: Imaging unavailable		3 (8)
Excluded: Incompatible CT protocols		7 (19)
Age in years: median (range)	56 (37–68)	
Gender	Male	21 (78)
	Female	6 (22)
Nivolumab response	Responders	19 (70)
	Non-responders	8 (30)
Tumor histology	Clear-cell	24 (89)
	Non-clear-cell	3 (11)
Prior nephrectomy	Yes	24 (89)
	No	3 (11)
Prior systemic therapy	Yes	24 (89)
	No	3 (11)
Lines of therapy	0	3
	1	14
	2	4
	3	3
	≥4	3
Prior treatment	Sunitinib	22
	Everolimus	8
	Axitinib	4
	Pazopanib	2
	Phase 1 trials	7
IMDC risk score	Good	8 (30)
	Intermediate	16 (60)
	Poor	3 (10)
Lesions contoured: 104		
Lymph nodes		62 (60)
Lung metastases		24 (23)
Kidney or adrenal metastases		18 (17)

CT: computed tomography; IMDC: International Metastatic RCC Database Consortium; ROI: region of interest.

analyzed using a SML radiomics application pipeline that has been previously validated.

Performance of radiomics signature

Lesion VOI contours were extracted using validated Neuroimaging Informatics Technology Initiative (NIfTI) software libraries. Each series consisted of a specific subject and set of lesion VOIs that were examined using the radiomics analysis software image display to confirm that: 1) the VOI contours were successfully extracted from the NIfTI files; and 2) their positions matched those of a lesion. No issues were found with the data set, and it was found to be suitable for radiomics texture analysis. The PROMISE contour bounded data were batch processed by the first stage of the radiomics application to generate the set of texture features to be used by the second stage radiomics SML application.

Supervised machine learning

The exhaustive iterative grid over the region of highest CV accuracy in the 3D space yielded a set of ROC curves as represented in Figs 4A and 4B for the pre-treatment and post-treatment groups, respectively. For the classifier trained on the baseline CT scans, 69% accuracy was achieved. For the classifier trained on the first post-treatment CT scans, 66% accuracy was achieved. The pre-specified level of sensitivity and specificity that was required for the analysis to be successful was 85%; on this basis, the pre- and post-treatment ROC curves do not demonstrate sufficient discriminatory ability to warrant further study.

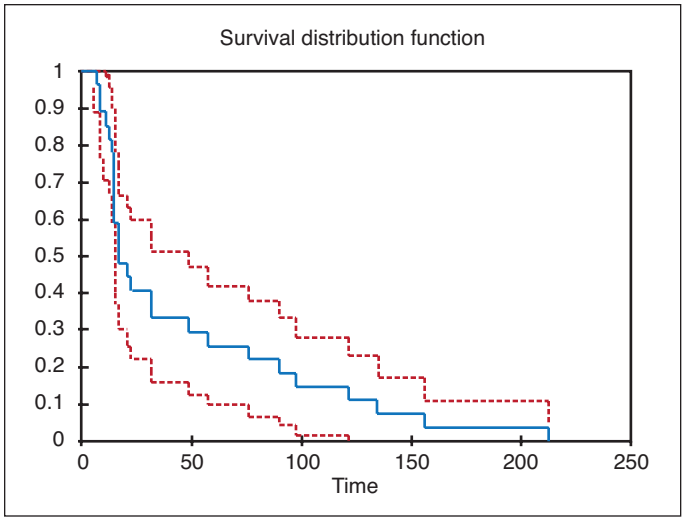

Fig. 1A. Kaplan-Meier curve of the progression-free survival (PFS) for the whole study population. Median PFS 10.8 months (range 1.4–48.8).

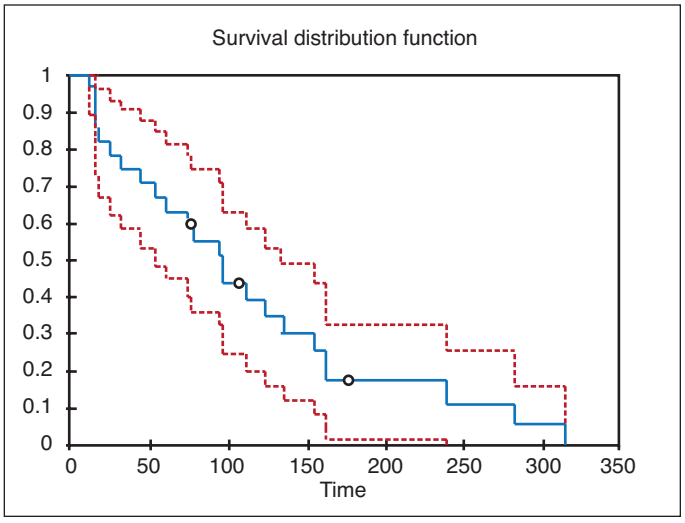

Fig. 1B. Kaplan-Meier curve of the overall survival (OS) for the whole study population. Median OS 26.2 months (range 3.1–72.5).

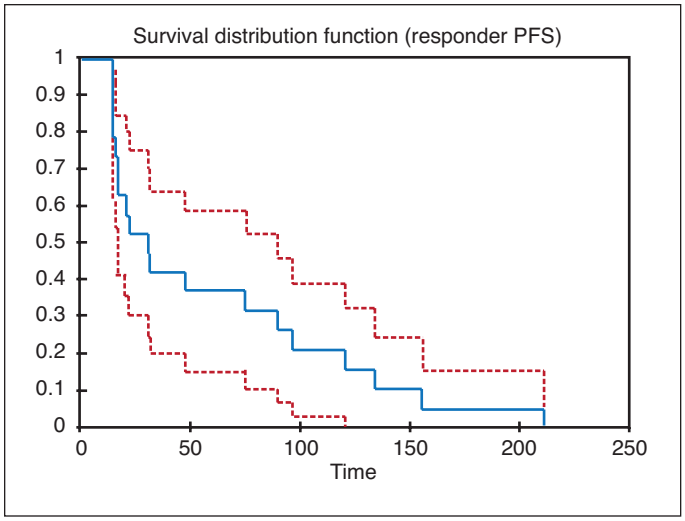

Fig. 2A. Kaplan-Meier curve of progression-free survival (PFS) for responders. Median PFS was 14 months (range 3.5–48.8 months).

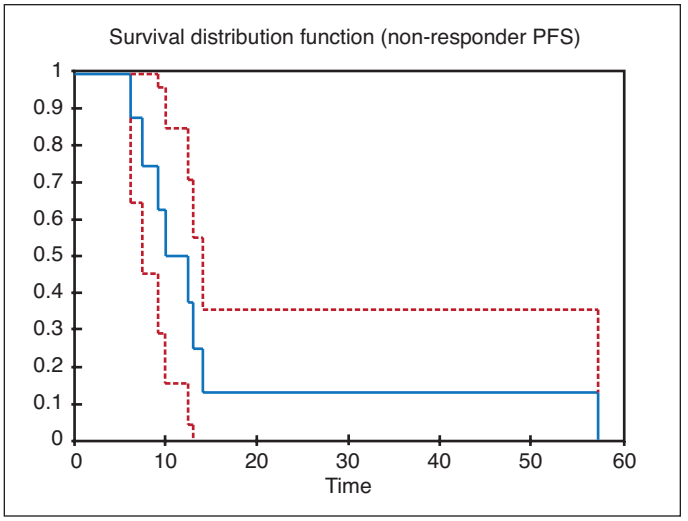

Fig. 2B. Kaplan-Meier curve of progression-free survival (PFS) for non-responders. Median PFS vs. 3.7 months (range 1.4–13.2).

Discussion

In patients with mRCC treated with ICI, we were not able to derive a radiomics signature that could predict for response or resistance to ICI. The pre- and post-treatment ROC curves are negative results for the radiomics analysis of the PROMISE data set. The current "as is" supervised machine learning set of algorithms were not able to discriminate significantly better than a binary classifier for a response in a malignant lesion. A reason for this might be that the user-defined texture features cannot significantly discriminate between ICI responder and non-responder classifications.

The patient population in this analysis was representative of the typical mRCC patient cohort that would be treated with ICI. The lesions contoured included lymph nodes, lung metastases, and renal metastases, which are typical of the metastases seen in this patient cohort. The OS in the responders was similar to what has been reported in the Checkmate-025 study; however, the PFS was much longer in the PROMISE responders compared to the Checkmate-025 cohort, which could be because without formal tumor measurements, physicians were more likely to continue patients beyond progression or at least call progression of disease later in the patients' treatment course.

There are certain limitations to the use of radiomics in general. For example, the textures that are sensitive to acquisition modes and reconstruction parameters are not recommended for radiomics applications, such as malignant and benign tissue differentiation.[18] Accurate delineation of tumor volumes is crucial for the computation of radiomic

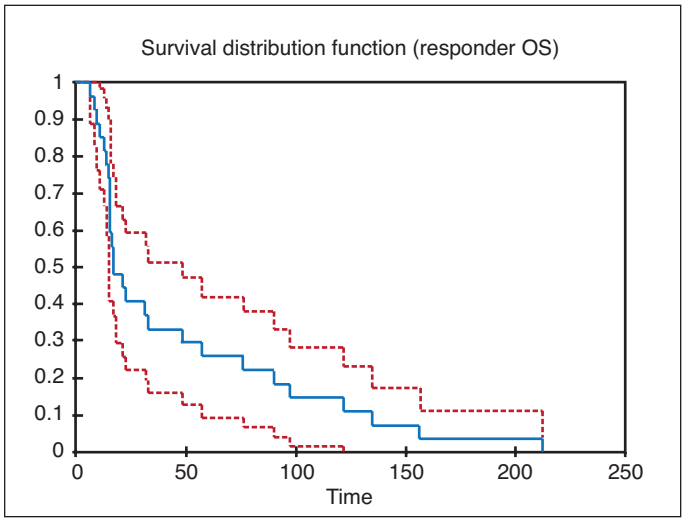

Fig. 3A. Kaplan-Meier curve of overall survival (OS) for responders. Median OS was 28.8 (range 3.7–72.5).

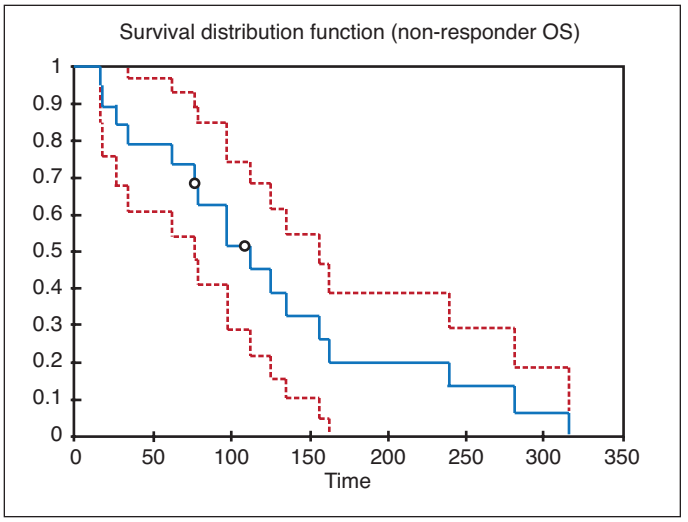

Fig. 3B. Kaplan-Meier curve for overall survival (OS) for non-responders. Median OS was 16.3 months (range 3.1–40.8).

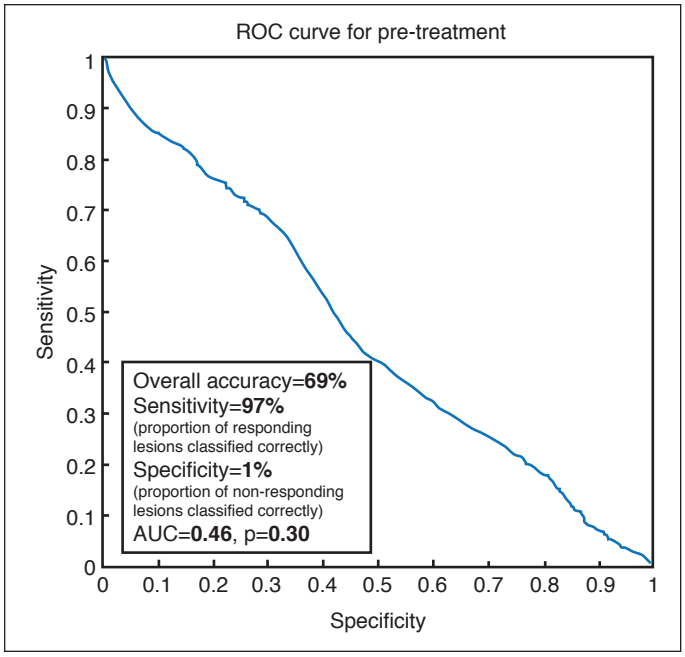

Fig. 4A. Pre-treatment. Specificity corresponds to the proportion of non-responding lesions classified correctly. Sensitivity corresponds to the proportion of responding lesions classified correctly. AUC: area under the curve.

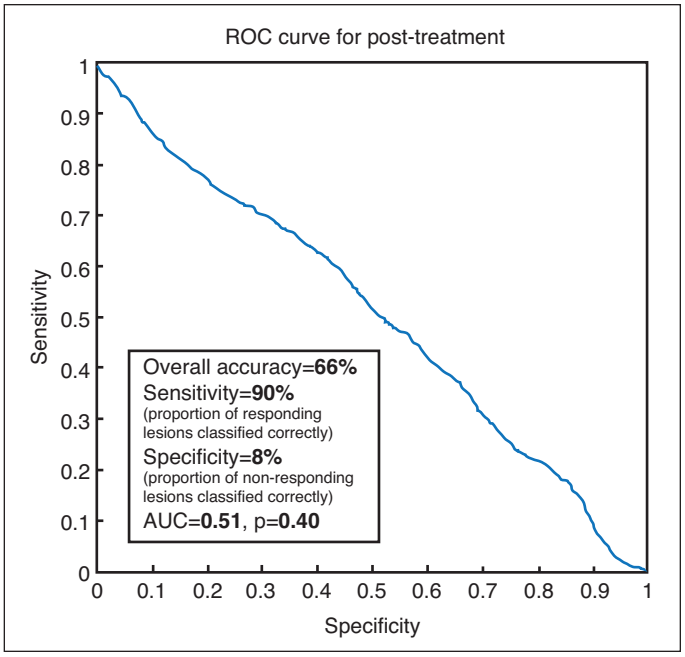

Fig. 4B. Post-treatment. Specificity corresponds to the proportion of non-responding lesions classified correctly. Sensitivity corresponds to the proportion of responding lesions classified correctly. AUC: area under the curve.

features; doing this manually is time-consuming and subject to inter-observer variability. Numerous studies have recommended automatic and semiautomatic methods of tumor volume delineation over manual contouring.[19, 20] We tried to account for this by having two investigators define the VOI, however, this approach may still have had inherent inaccuracies that could have been resolved by an automated process. Although tumor heterogeneity can potentially be quantified using radiomics features extracted from medical imaging, many features are unstable between imaging scans, which would mean that a large number of features may be unreliable.[21,22] Datasets need to consist of 10–15 patients per feature to reduce the false discovery rate, necessitating the use of larger datasets.[23] Optimal cutoff values of radiomic features are often used to stratify patients into two risk groups for KM survival analysis; however, searching for the optimal cutoff values through testing multiple thresholds can increase the likelihood of obtaining statistically significant but spurious results. As the optimum cutoff value can vary in different datasets, single-study results may not be reproducible in other patient populations. Independent validation datasets are required to confirm the prognostic value of the same radiomics features to avoid false-positive results.[24,25]

Recent studies have confirmed the utility of radiomics across numerous cancer types (lung cancer;[25-32] head and neck cancer;[25,27,33,34] glioblastoma;[35-38] esophageal cancer;[9,39-41] rectal cancer;[42] hepatocellular carcinoma;[43] prostate cancer;[44] RCC;[45] soft tissue sarcoma;[46] and germ cell tumors[47]) using various imaging modalities. In one study, radiomics features for predicting the survival of patients with lung cancer were found to be distinct from those for head and neck cancer, highlighting the need to develop tumor-specific signatures.[27] In general, most studies have explored correlates of survival, gene expression, or molecular pathway aberrations. Several studies investigated predictive signatures for pathological response to neoadjuvant chemoradiotherapy.[9,19,29,39-42] At this stage, the role of radiomics is still emerging, and radiomics has not been integrated into clinical practice, as signatures have not yet been independently validated and the complexity of deriving the signature may make it difficult to implement outside of centers that do not have the computational algorithms to calculate such signatures.

The current study does have some important limitations. It is a retrospective, single-institution analysis that used a selected patient sample without an external validation cohort. The sample size was small in this pilot study because of the time required for manual contouring of primary kidney lesions and metastatic lesions from different sites. A larger sample size would have been prohibitive without automation. We do not know if adding further patients would potentially change the results seen. Radiomics is a technically challenging and time-consuming approach and so is unlikely to be usable outside larger tertiary cancer centers without improvements in automated contouring of ROIs.

Conclusions

The study of radiomics could be continued in mRCC as new methods become available, such as additional novel texture feature measures added to the existing standard set, which may improve discriminating capability between the ICI non-responder and responder classifications. Furthermore, radiomics in mRCC requires substantially more data, with a higher number of patients for the analysis to have a greater chance of success. The use of more advanced supervised machine learning techniques, such as convolutional neural networks, which learn high-level features, is required. Unsupervised deep learning, automated volume delineation or variational auto-encoders, which would sort the images into different regions of low-dimensional space based on intrinsic image properties, are possible technological innovations that may enhance the development of a radiomics signature for mRCC. If these advances can be integrated into such an analysis, then a radiomics signature for mRCC patients treated with immunotherapy may be more feasible.

Competing interests: Dr. Sim has received research funding from Abbvie and Bristol-Myers Squibb; Dr. Metser has had a consulting or advisory role with Point Biopharm Inc. Dr. Sacher has been a consultant or advisor for, has received honoraria from, or has participated in clinical trials supported by Amgen, AstraZeneca, Bayer, Bristol Myers Squibb, Genentech–Roche, GlaxoSmithKline, KisoJi Biotechnology, Merck, Pfizer, Spectrum, and Tesaro. Dr. Sridhar has received compensation from Astellas, AstraZeneca, Bayer, BMS, Merck, Pfizer, and Roche for service as a consultant, and has received research funding from Janssen and Sanofi. Dr. Hansen has received honoraria from AstraZeneca/MedImmune, Bristol-Myers Squibb, GlaxoSmithKline, Merck, Novartis, and Pfizer; has served in a consulting or advisory role for Boehringer Ingelheim, Boston Biomedical, Bristol-Myers Squibb, GlaxoSmithKline, Merck, Novartis, and Roche/Genetech; has received research funding from Boehringer Ingelheim, Bristol-Myers Squibb, GlaxoSmithKline, Janssen, Karyopharm Therapeutics, Merck, Novartis, and Roche/Genetech. The remaining authors do not report any competing personal or financial interests related to this work.

Acknowledgment/funding: This work was supported by the Genitourinary Medical Oncologists of Canada (GUMOC) Astellas Research Grant.

This paper has been peer-reviewed.

References

1. Motzer RJ, Escudier B, McDermott DF, et al. Nivolumab vs. everolimus in advanced renal cell carcinoma. *N Engl J Med* 2015;373:1803-13. https://doi.org/10.1056/NEJMoa1510665
2. Motzer RJ, Penkov K, Haanen J, et al. Avelumab plus axitinib vs. sunitinib for advanced renal cell carcinoma. *N Engl J Med* 2019;380:1103-15. https://doi.org/10.1056/NEJMoa1816047
3. Motzer RJ, Tannir NM, McDermott DF, et al. Nivolumab plus ipilimumab vs. sunitinib in advanced renal cell carcinoma. *N Engl J Med* 2018;378:1277-90. https://doi.org/10.1056/NEJMoa1712126
4. Rini BI, Plimack ER, Stus V, et al. Pembrolizumab plus axitinib vs. sunitinib for advanced renal cell carcinoma. *N Engl J Med* 2019;380:1116-27. https://doi.org/10.1056/NEJMoa1816714
5. Lambin P, Rios-Velazquez E, Leijenaar R, et al. Radiomics: Extracting more information from medical images using advanced feature analysis. *Eur J Cancer* 2012;48:441-6. https://doi.org/10.1016/j.ejca.2011.11.036
6. Kumar V, Gu Y, Basu S, et al. Radiomics: The process and the challenges. *Magn Reson Imaging* 2012;30:1234-48. https://doi.org/10.1016/j.mri.2012.06.010
7. Eisenhauer EA, Therasse P, Bogaerts J, et al. New response evaluation criteria in solid tumours: Revised RECIST guideline (version 1.1). *Eur J Cancer* 2009;45:228-47. https://doi.org/10.1016/j.ejca.2008.10.026
8. Wolchok JD, Hoos A, O'Day S, et al. Guidelines for the evaluation of immune therapy activity in solid tumors: Immune-related response criteria. *Clin Cancer Res* 2009;15:7412-20. https://doi.org/10.1158/1078-0432.CCR-09-1624
9. Tixier F, Le Rest CC, Hatt M, et al. Intratumor heterogeneity characterized by textural features on baseline 18F-FDG PET images predicts response to concomitant radiochemotherapy in esophageal cancer. *J Nucl Med* 2011;52:369-78. https://doi.org/10.2967/jnumed.110.082404
10. Haralick RM, Shanmugam K, Dinstein IH. Textural features for image classification. *IEEE Transact Syst Man Cybernetics* 1973;3:610-21. https://doi.org/10.1109/TSMC.1973.4309314
11. Amadasun M, King R. Textural features corresponding to textural properties. *IEEE Transact Syst Man Cybernetics* 1989;19:1264-74. https://doi.org/10.1109/21.44046
12. Loh H, Leu J, Luo RC. The analysis of natural textures using run length features. *IEEE Transact Indust Electronics* 1988;35:323-8. https://doi.org/10.1109/41.192665
13. Thibault G, Fertil B, Navarro C, et al. Texture indexes and gray level size zone matrix application to cell nuclei nlassification. 2009. Available at: https://www.researchgate.net/publication/255609273_Texture_Indexes_and_Gray_Level_Size_Zone_Matrix_Application_to_Cell_Nuclei_Classification. Accessed Sept. 24, 2021.
14. Chang CC, Lin CJ. LIBSVM: A library for support vector machines. *ACM Trans Intell Syst Technol* 2011;2:1-27. https://doi.org/10.1145/1961189.1961199
15. Chen YW. Lin CJ. Combining SVMs with various feature selection strategies. In: Guyon I, Nikravesh M, Gunn S, Zadeh LA (eds), Feature Extraction Studies in Fuzziness and Soft Computing, vol 207 Springer, Berlin, Heidelberg. (2006) 315-24. https://doi.org/10.1007/978-3-540-35488-8_13
16. Golland P, Fischl B. Permutation tests for classification: Towards statistical significance in image-based studies. *Inf Process Med Imag* 2003;18:330-41. https://doi.org/10.1007/978-3-540-45087-0_28
17. Heng DY, Wells JC, Rini BI, et al. Cytoreductive nephrectomy in patients with synchronous metastases from renal cell carcinoma: Results from the International Metastatic Renal Cell Carcinoma Database Consortium. *Eur Urol* 2014;66:704-10. https://doi.org/10.1016/j.eururo.2014.05.034
18. Galavis PE, Hollensen C, Jallow N, et al. Variability of textural features in FDG PET images due to different acquisition modes and reconstruction parameters. *Acta Oncol* 2010;49:1012-6. https://doi.org/10.3109/0284186X.2010.498437
19. Yip SS, Coroller TP, Sanford NN, et al. Use of registration-based contour propagation in texture analysis for esophageal cancer pathologic response prediction. *Phys Med Biol* 2016;61:906-22. https://doi.org/10.1088/0031-9155/61/2/906
20. Parmar C, Rios Velazquez E, Leijenaar R, et al. Robust radiomics feature quantification using semiautomatic volumetric segmentation. *PLoS One* 2014;9:e102107. https://doi.org/10.1371/journal.pone.0102107
21. Balagurunathan Y, Gu Y, Wang H, et al. Reproducibility and prognosis of quantitative features extracted from CT Images. *Transl Oncol* 2014;7:72-87. https://doi.org/10.1593/tlo.13844
22. Tixier F, Hatt M, Le Rest CC, et al. Reproducibility of tumor uptake heterogeneity characterization through textural feature analysis in 18F-FDG PET. *J Nucl Med* 2012;53:693-700. https://doi.org/10.2967/jnumed.111.099127
23. Chalkidou A, O'Doherty MJ, Marsden PK. False discovery rates in PET and CT studies with texture features: A systematic review. *PLoS One* 2015;10:e0124165. https://doi.org/10.1371/journal.pone.0124165
24. Yip SS, Aerts HJ. Applications and limitations of radiomics. *Phys Med Biol* 2016;61:R150-66. https://doi.org/10.1088/0031-9155/61/13/R150
25. Aerts HJ, Velazquez ER, Leijenaar RT, et al. Decoding tumour phenotype by noninvasive imaging using a quantitative radiomics approach. *Nat Commun* 2014;5:4006. https://doi.org/10.1038/ncomms5006
26. Aerts HJ, Grossmann P, Tan Y, et al. Defining a radiomic response phenotype: A pilot study using targeted therapy in NSCLC. *Sci Rep* 2016;6:33860. https://doi.org/10.1038/srep33860
27. Parmar C, Leijenaar RT, Grossmann P, et al. Radiomic feature clusters and prognostic signatures specific for lung and head & neck cancer. *Sci Rep* 2015;5:11044. https://doi.org/10.1038/srep11044
28. Ganeshan B, Abaleke S, Young RC, et al. Texture analysis of non-small cell lung cancer on unenhanced computed tomography: Initial evidence for a relationship with tumour glucose metabolism and stage. *Cancer Imaging* 2010;10:137-43. https://doi.org/10.1102/1470-7330.2010.0021
29. Cook GJ, Yip C, Siddique M, et al. Are pretreatment 18F-FDG PET tumor textural features in non-small cell lung cancer associated with response and survival after chemoradiotherapy? *J Nucl Med* 2013;54:19-26. https://doi.org/10.2967/jnumed.112.107375
30. Ganeshan B, Goh V, Mandeville HC, et al. Non-small cell lung cancer: Histopathological correlates for texture parameters at CT. *Radiology* 2013;266:326-36. https://doi.org/10.1148/radiol.12112428

31. Coroller TP, Grossmann P, Hou Y, et al. CT-based radiomic signature predicts distant metastasis in lung adenocarcinoma. *Radiother Oncol* 2015;114:345-50. https://doi.org/10.1016/j.radonc.2015.02.015
32. Huang Y, Liu Z, He L, et al. Radiomics signature: A potential biomarker for the prediction of disease-free survival in early-stage (I or II) non-small cell lung cancer. *Radiology* 2016;281:947-57. https://doi.org/10.1148/radiol.2016152234
33. Cheng NM, Fang YH, Lee LY, et al. Zone-size nonuniformity of 18F-FDG PET regional textural features predicts survival in patients with oropharyngeal cancer. *Eur J Nucl Med Mol Imaging* 2015;42:419-28. https://doi.org/10.1007/s00259-014-2933-1
34. Prawira A, Dufort P, Halankar J, et al. Development of a predictive radiomics signature for response to immune checkpoint inhibitors (ICIs) in patients with recurrent or metastatic squamous cell carcinoma of the head and neck (RM-SCCHN) *Ann Oncol* 2016;27. https://doi.org/10.1093/annonc/mdw376.08
35. Jamshidi N, Diehn M, Bredel M, et al. Illuminating radiogenomic characteristics of glioblastoma multiforme through integration of MR imaging, messenger RNA expression, and DNA copy number variation. *Radiology* 2014;270:1-2. https://doi.org/10.1148/radiol.13130078
36. Gutman DA, Dunn WD JR, Grossmann P, et al. Somatic mutations associated with MRI-derived volumetric features in glioblastoma. *Neuroradiology* 2015;57:1227-37. https://doi.org/10.1007/s00234-015-1576-7
37. Gevaert O, Mitchell LA, Achrol AS, et al. Glioblastoma multiforme: Exploratory radiogenomic analysis by using quantitative image features. *Radiology* 2014;273:168-74. https://doi.org/10.1148/radiol.14131731
38. Diehn M, Nardini C, Wang DS, et al. Identification of non-invasive imaging surrogates for brain tumor gene-expression modules. *Proc Natl Acad Sci U S A* 2008;105:5213-8. https://doi.org/10.1073/pnas.0801279105
39. Zhang H, Tan S, Chen W, et al. Modeling pathologic response of esophageal cancer to chemoradiation therapy using spatial-temporal 18F-FDG PET features, clinical parameters, and demographics. *Int J Radiat Oncol Biol Phys* 2014;88:195-203. https://doi.org/10.1016/j.ijrobp.2013.09.037
40. van Rossum PS, Fried DV, Zhang L, et al. The incremental value of subjective and quantitative assessment of 18F-FDG PET for the prediction of pathologic complete response to preoperative chemoradiotherapy in esophageal cancer. *J Nucl Med* 2016;57:691-700. https://doi.org/10.2967/jnumed.115.163766
41. Yip SS, Coroller TP, Sanford NN, et al. Relationship between the temporal changes in positron emission tomography imaging-based textural features and pathological response and survival in esophageal cancer patients. *Front Oncol* 2016;6:72. https://doi.org/10.3389/fonc.2016.00072
42. Metser U, Murphy G, Halankar J, et al. Multiparameteric PET-MR assessment of response to neoadjuvant chemoradiotherapy in locally advanced rectal cancer: PET, MR, PET-MR and tumor texture analysis: A pilot study. *Adv Molec Imag* 2015;5:49-60. https://doi.org/10.4236/ami.2015.53005
43. Segal E, Sirlin CB, Ooi C, et al. Decoding global gene expression programs in liver cancer by non-invasive imaging. *Nat Biotechnol* 2007;25:675-80. https://doi.org/10.1038/nbt1306
44. Stoyanova R, Takhar M, Tschudi Y, et al. Prostate cancer radiomics and the promise of radiogenomics. *Transl Cancer Res* 2016;5:432-47. https://doi.org/10.21037/tcr.2016.06.20
45. Shinagare AB, Vikram R, Jaffe C, et al. Radiogenomics of clear cell renal cell carcinoma: Preliminary findings of The Cancer Genome Atlas-Renal Cell Carcinoma (TCGA-RCC) Imaging Research Group. *Abdom Imaging* 2015;40:1684-92. https://doi.org/10.1007/s00261-015-0386-z
46. Vallieres M, Freeman CR, Skamene SR, et al. A radiomics model from joint FDG-PET and MRI texture features for the prediction of lung metastases in soft-tissue sarcomas of the extremities. *Phys Med Biol* 2015;60:5471-96. https://doi.org/10.1088/0031-9155/60/14/5471
47. Lewin J, Dufort P, Halankar J, et al. Applying radiomics to predict pathology of postchemotherapy retroperitoneal nodal masses in germ cell tumors. *JCO Clin Cancer Inform* 2018;2:1-12. https://doi.org/10.1200/CCI.18.00004

Correspondence: Dr. Aaron Hansen, Division of Medical Oncology and Hematology, Princess Margaret Cancer Centre, UHN, Toronto, ON, Canada; aaron.hansen@uhn.ca